Helium desorption from Fe and V by atomic diffusion and bubble migration

R. Vassen, H. Trinkaus, and P. Jung
Institut für Festkörperforschung, Forschungszentrum Jülich, Postfach 1913, D-5170 Jülich, Germany
(Received 22 January 1991)

Thermal helium desorption from homogeneously implanted iron and vanadium foils was investigated during linear heating and isothermal annealing, respectively. The isothermal experiments showed an initial period with a square-root dependence of the desorbed helium on time, characteristic of atomic helium diffusion, followed by a reduction of desorption due to clustering. The substitutional helium atoms migrate by a dissociative mechanism, with dissociation energies of 1.4 ± 0.3 eV for both metals. Up to temperatures of 600 K (Fe) and 700 K (V), retrapping was dominated by irradiation-induced vacancies. At higher temperatures diffusion times became unmeasurably small. Retention of helium in the specimens indicated that di-helium clusters are stable up to 673 K in Fe and up to 773 K in V. Desorption after clustering was analyzed by comparison with models of bubble coarsening. The vanadium results were best described by bubble migration via surface diffusion at all temperatures investigated (573–1173 K), while the iron data from 900 to 1184 K indicated bubble migration by volume diffusion as the prevalent coarsening mechanism.

I. INTRODUCTION

Noble gases in metals have great effects on material properties not only in nuclear technology [fission gases in nuclear fuels, helium from (n,α) reactions in fusion reactor materials, ^{3}He in materials for tritium storage], but appear also in materials produced by hot isostatic pressing or by sputtering. These technical aspects, as well as basic scientific interest, have prompted extensive investigations on the behavior of noble gases, especially of helium, in materials.

In the present investigation α particles were homogeneously implanted in Fe and V foils of 2.5–42 μm thickness, up to concentrations ranging from 10^{-3} to 5 at. ppm. The low thicknesses and concentrations were chosen to avoid clustering, at least during implantation and at the beginning of the subsequent desorption experiment. Desorption measurements were not only employed to study atomic diffusion, but also to analyze, on the basis of simple models, the coarsening of submicroscopic clusters or bubbles.

II. EXPERIMENTAL DETAILS

Specimen material was obtained from Goodfellow, Cambridge, UK. The iron foils of 2.5-, 5.7-, and 20-μm thickness had nominal impurities of 99.85%, 99.95%, and 99.99%, respectively. They were annealed for 1 h at 1113 K in a quartz tube in a vacuum of 10^{-6} mbar to remove cold working and to produce a stable grain structure. By this treatment the room-to-helium-temperature resistivity ratio increased from about 31 to 71. The vanadium foils of 5, 10, 20, and 42 μm had impurities of 99.8% and room-to-nitrogen-temperature resistivity ratios (RNR) of about 6. While it was not possible to anneal the 5-μm foils because of mechanical instability, the 10- and 20-μm foils were annealed for $\frac{1}{2}$ h at 1673 K by inductive heating in 2×10^{-9} mbar vacuum. This treatment slightly reduced RNR to about 5.4. The 42-μm foils were annealed by direct-current heating (10 min at 2073 K) in an 8×10^{-9} mbar vacuum, yielding a slight improvement of RNR to 6.3. This improvement was probably mainly due to the faster cooling at intermediate temperatures.

The specimens were implanted at the Jülich compact cyclotron with 28-MeV α particles. Lateral homogeneity was achieved by wobbling the beam at about 300 cps across an aperture. The energy of the α particles was varied by a rotating degrader wheel to obtain homogeneous helium concentration across the specimen thickness. On the circumference of the degrader wheel 51 aluminum foils were mounted with thicknesses from 18 to 281 μm. The thicknesses of the Al foils were chosen in a way that the steps in the mean implantation depths was less than the standard deviation of the implantation profiles (≈2 μm). This gave a ripple of the implanted helium concentration of less than 1%. The degrader wheel was optimized for implantation in gold. For other materials slight inhomogeneities occurred due to differences in stopping power. In Fig. 1 measured concentrations in a stack of 6-μm iron foils are compared to calculations using stopping powers from the literature.[1] When the first and the last 10 μm of the range was omitted, the inhomogeneity even in a 20-μm foil was less than ±2%. More details of the implantation apparatus are given in Refs. 2 and 3.

Pieces of about 2×3 mm^2 of the implanted specimens were degassed in a furnace in a closed UHV desorption apparatus.[2,3] During degassing a vacuum of about 10^{-7} mbar was maintained in the system by a titanium sublimation pump. The helium partial pressure was monitored by a quadrupole mass spectrometer. The furnace was heated by a constant rate of typically 0.83 K/s (linear ramping) or at constant temperature (isothermal). At the

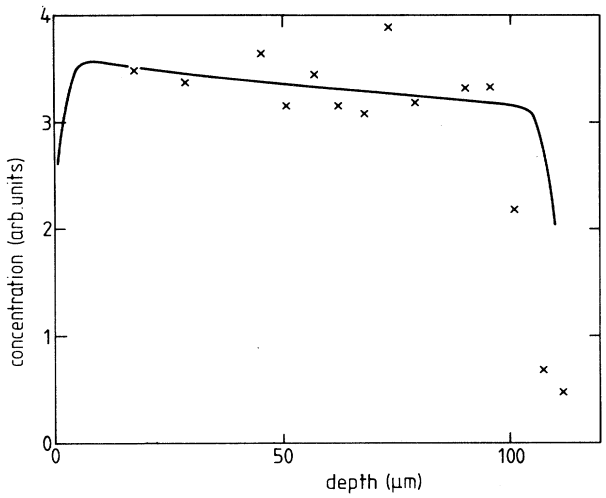

FIG. 1. Measured helium concentrations in 6-μm iron foils after implantation with degraded 28-MeV α particles. The solid line indicates stopping-power calculations (see Ref. 1).

end of each experiment the total helium content was determined by melting the specimen.

III. THEORETICAL BACKGROUND

A. Diffusion and early stage of clustering

When energetic helium ions are implanted into metals at intermediate temperatures, the mobile interstitial helium atoms will soon be strongly trapped in vacancies produced during implantation. For most metals this behavior is characteristic for temperatures from about 100 to at least 500 K. In this temperature range implantation will produce substitutional helium atoms and displacement defects. While the self-interstitial atoms will be incorporated in small clusters, at dislocations or at grain boundaries, the vacancies, depending on temperature, may still persist as atomic defects. These are the conditions at the beginning of the desorption experiment (see, e.g., Ref. 4).

The diffusion equation for desorption from a homogeneously loaded foil has no simple analytical solution. Only for small times, at which the two surfaces act independently, the released fraction can be approximated as a function of initial helium concentration c_0 and specimen thickness d by (see, e.g., Ref. 5)

$$\frac{c_0-c}{c_0}=\left[\frac{16D_{\mathrm{He}}t}{\pi d^2}\right]^{1/2}, \quad \text{for } \frac{c_0-c}{c_0}\leq 0.5 \ . \tag{1}$$

Substitutional helium may become mobile by exchanging sites with an adjacent vacancy (vacancy mechanism) or by dissociating from its lattice position and migrating interstitially until it is trapped in another vacancy (dissociative mechanism). Experiments in Ref. 6 showed that a limit of the diffusion coefficients for the vacancy mechanism is given by

$$D_V c_V \leq D_{\mathrm{He}} \ , \tag{2}$$

where D_V is the vacancy diffusivity. If the vacancy concentration c_V corresponds to thermal equilibrium, this lower limit is given by the self-diffusion coefficient. If the implantation-induced vacancies prevail and if the vacancy annihilation is sink controlled, then c_V is proportional to the implanted helium concentration c_0. As a result D_{He} will become proportional to c_0 with an activation energy equal to the vacancy migration energy. For the dissociative mechanism one obtains[6]

$$D_{\mathrm{He}}=(\beta/6)\nu_d r_i^2/c_v \ , \tag{3}$$

where $\nu_d=\nu_0\exp(-E^{\mathrm{dis}}/kT)$ is the dissociation frequency, r_i is the jump distance on interstitial sites, and β is a geometry factor. If thermal vacancies dominate, the activation energy for helium diffusion by the dissociation mechanism is given by the difference of the dissociation energy (E^{dis}) and the vacancy formation energy (E_v^f). If implantation-induced vacancies prevail, D_{He} has an activation energy E^{dis} and becomes reciprocal to c_0.

The $\sqrt{t}$ law in Eq. (1) is only valid as long as the helium atoms diffuse freely without clustering. In the simplest model of agglomeration, we assumed that the atomic concentration c_f of freely migrating helium in the bulk is reduced only by the formation of immobile di-helium complexes (cf. Ref. 7):

$$\frac{dc_f}{dt}=-\frac{8\pi R D_{\mathrm{He}} c_f^2}{\Omega} \ , \tag{4}$$

giving

$$c_f/c_0=(1+8\pi D_{\mathrm{He}} R c_0 t/\Omega)^{-1} \ , \tag{5}$$

where R is the interaction distance and Ω is the atomic volume of the matrix atoms. To estimate the desorption under this condition, we assume an approximate concentration profile as shown in Fig. 2. In this case Fick's law for the helium current density j_1 through one specimen surface reads

$$j_1=aD_{\mathrm{He}}c_f/(y\Omega) \ , \tag{6a}$$

whereas helium conservation requires

$$j_1=a\frac{c_f}{2\Omega}\frac{dy}{dt} \ . \tag{6b}$$

The numerical factor a, which would be equal to 1 for the trapezoid in Fig. 2, is added to account for the difference to the real diffusion profile. Integration of Eqs. (6a) and (6b) yields

$$y=2\sqrt{D_{\mathrm{He}}t} \ . \tag{7}$$

The desorbed fraction from both surfaces is then given by

$$\frac{c_0-c}{c_0}=\frac{\Omega}{c_0 d}\int 2j_1\,dt \ . \tag{8}$$

When Eqs. (6a) and (7) are inserted in (8), the solution for $c_f=c_0$, i.e., without clustering, can be compared to Eq. (1), yielding $a=2/\sqrt{\pi}$. Using this value as an estimate, integration of Eq. (8) gives

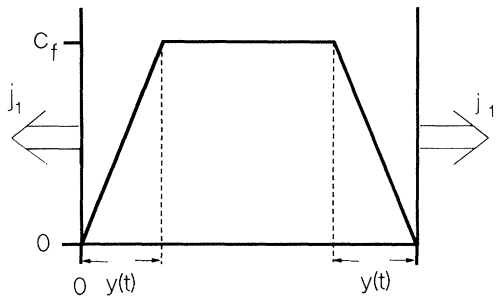

FIG. 2. Simplified concentration profile during desorption.

$$\frac{c_0-c}{c_0}=\left[\frac{2\Omega}{\pi^2 R c_0 d^2}\right]^{1/2}\arctan\sqrt{8\pi D_{\mathrm{He}} R c_0 t/\Omega}\ . \tag{9}$$

The total fraction of helium desorbed by free atomic diffusion before clustering is obtained by the $t=\infty$ limit of expression (9):

$$\left[\frac{c_0-c}{c_0}\right]_c=0.6\frac{\sqrt{\Omega/2R}}{d\sqrt{c_0}}\ . \tag{10}$$

The factor 0.6 results from numerical calculations[8] when additional trapping of migrating helium atoms by di-helium clusters is taken into account. These calculations also show that the dependence of $[(c_0-c)/c_0]_c$ on d and c_0 remains almost unchanged when di-helium clusters are allowed to dissociate and only larger clusters become stable. Only the absolute amount of $[(c_0-c)/c_0]_c$ is increased in the latter case. Therefore, comparison of Eq. (10) to experimental $[(c_0-c)/c_0]_c$ data, i.e., the fraction of helium desorption obeying the $\sqrt{t}$ dependence, gives an indication of the minimum size of stable clusters.

B. Desorption during bubble coarsening

After agglomeration helium desorption can continue by two mechanisms: migration of the clusters or bubbles or helium dissociation from bubbles. Bubbles may migrate by diffusion of lattice atoms along their surfaces, through the matrix, or through the gas-filled bubble. The diffusion coefficient D_B of the bubble is proportional to the diffusion coefficient of the underlying diffusion process and decreases with increasing bubble radius r_B according to

$$D_B=\beta_i D_i/r_B^n\ . \tag{11}$$

The respective parameters for volume diffusion ($D_i=D_{\mathrm{VD}}$) are $\beta_{\mathrm{VD}}=3\Omega/4\pi$ and $n=3$, and for surface diffusion ($D_i=D_{\mathrm{SD}}$) in a surface layer of thickness b, $\beta_{\mathrm{SD}}=3b\Omega/(2\pi)$ and $n=4$.[9] The diffusion coefficient will decrease with time as the bubbles grow by coalescence. It must, however, be considered that the surface diffusion coefficients in small bubbles may differ from conventional D_{SD} values because of the strong curvature of the surface. On the other hand, by reason of this strong curvature, ledge nucleation must not be taken into consideration as a limiting factor for the migration of small bubbles.

An understanding of desorption during bubble coarsening requires knowledge of bubble coarsening within an unlimited volume. Even in this simpler case the evolution of a given initial bubble-size distribution is described by a large system of coalescence equations.[10] Following Ref. 11, we approximate the evolution of the bubble number density c_B analogous to Eq. (4):

$$\frac{dc_B}{dt}=-8\pi D_B r_B c_B^2\ , \tag{12}$$

where r_B is some representative average of the bubble radii. Note that the interaction distance is assumed as $2r_B$. The apparent reduction of the rate in Eq. (12) by a factor of 2 as compared to Eq. (4) takes into account that, as by the removal of two bubbles in a coalescence event, another bubble is formed.

Since after the diffusional stage the overwhelming fraction of helium is contained in clusters or bubbles, the requirement of helium conservation in the bulk yields an additional relation between c_B and r_B:

$$(4\pi/3)\ r_B^3 c_B \Omega/v_{\mathrm{He}}(p)=c_0\ . \tag{13}$$

In order to use this expression the atomic volume of helium v_{He} or the corresponding pressure p (both related by the equation of state) within the bubbles must be known. If, for instance, the vacancy concentration corresponds to thermal equilibrium and the bubbles are in local equilibrium with this vacancy concentration, the pressure in the bubbles is given by

$$p=2\gamma_B/r_B\ , \tag{14}$$

where γ_B is the surface free energy of the bubble. The other extreme case would be that the total amount of vacancies, most of which is also contained in bubbles, is conserved during coarsening, meaning that the volume v_{He} available for helium remains constant. If in the first case ideal gas behavior is assumed ($pv_{\mathrm{He}}=kT$), combination of Eqs. (12)–(14) yields

$$r_B=r_c\left[1+\frac{3(n+1)\beta_i kTc_0}{2\gamma_B\Omega r_c^{(n+1)}}D_i(t-t_c)\right]^{1/(n+1)}\ , \tag{15}$$

where the suffix c denotes the beginning of coalescence at time t_c with average bubble radius r_c. For the extremely high equilibrium pressures occurring in the very small bubbles of the present experiment, the assumption of constant v_{He}, which is also realized in the second case of constant total vacancy concentration, seems more appropriate than the assumption of ideal gas behavior. For constant v_{He} Eqs. (12) and (13) yield

$$r_B=r_c\left[1+\frac{3\delta_i v_{\mathrm{He}}c_0}{\pi r_c^{(n+2)}}D_i(t-t_c)\right]^{1/(n+2)}\ , \tag{16}$$

with $\delta_{\mathrm{VD}}=\frac{5}{2}$ and $\delta_{\mathrm{SD}}=6\Omega^{1/3}$. For $t\to\infty$ the dependence of r_B on t and the other parameters is confirmed by a more rigorous treatment in Ref. 12.

Near to a surface, bubble migration results in addition-

TABLE I. Parameters to describe helium desorption during bubble migration by various diffusion mechanisms in Eq. (19).

Diffusion	Gas law	A	B	m
Volume	Ideal gas	$\frac{32 r_c \gamma_B \Omega}{3\pi k T c_0 d^2}$	$B_{VD}=\frac{9kTc_0}{2\pi\gamma_B r_c^4}$	$\frac{1}{4}$
Surface	Ideal gas		$B_{SD}=B_{VD}5\Omega^{1/3}/2r_c$	$\frac{1}{5}$
Volume	Constant volume	$\frac{4r_c^2\Omega}{\pi v_{He} c_0 d^2}$	$B_{VD}=\frac{15 v_{He} c_0}{2\pi r_c^5}$	$\frac{2}{5}$
Surface	Constant volume		$B_{SD}=B_{VD}12\Omega^{1/3}/5r_c$	$\frac{1}{3}$

al gas desorption associated with the evolution of a depleted zone. From a theoretical point of view this complicates the problem substantially. Therefore a simplified procedure will be used, analogous to the one presented above for helium diffusion with concurrent formation of immobile di-helium. As in Eq. (6) the helium current density carried by bubbles through one surface is approximated by

$$j_1 = D_B c_0 / y\Omega \ , \tag{17}$$

implying that in the plateau in Fig. 2 virtually all of the original helium concentration is retained in bubbles. y is defined analogously to Eq. (7),

$$\left[\frac{y}{2}\right]^2 = \int D_B(t)\,dt \ , \tag{18}$$

and desorption is described by Eq. (8). Integration yields a general expression for the fraction of desorbed helium[3]:

$$\left[\frac{c_0-c}{c_0}\right]^2 - \left[\frac{c_0-c}{c_0}\right]_c^2 = A\{[1+BD_i(t-t_c)]^m - 1\} \ . \tag{19}$$

The parameters A, B, and n for the various mechanisms are given in Table I. Note that for $t \to \infty$ the functional dependences in Eq. (19) are confirmed by a more rigorous treatment in Ref. 12. The transient is crudely accounted for by an appropriate choice of the initial condition.

An alternative mechanism for desorption of helium after bubble formation is dissociation from bubbles. As dissociation is faster from small bubbles, due to their higher pressure, and as helium will be recaptured preferentially at large bubbles, the bubble structure will coarsen (Ostwald ripening). This in turn will cause a slowing down of the desorption rate. As the present investigation[3] gave no indication of Ostwald ripening in Fe and V, it will not be treated here in detail.

IV. RESULTS

Figure 3 shows examples of released fractions of implanted helium during isothermal degassing of iron. Up to about 700 K an initial part can be resolved which shows a $\sqrt{t}$ dependence in accordance to Eq. (1). The diffusion coefficients are reciprocal to c_0 up to 600 K (Fig. 4), while around 670 K this reciprocity is no longer precisely fulfilled, causing significant scatter of data. The fractional release by atomic diffusion at different temperatures is given in Fig. 5 as function of $d\sqrt{c_0}$, according to Eq. (10). Figure 6 shows surface diffusion coefficients derived by Eq. (19) from desorption measurements beyond the $\sqrt{t}$ regime. Helium diffusion coefficient in vanadium derived from linear heating (Fig. 7) and isothermal (Fig. 8) experiments are also reciprocal to c_0 (Fig. 9). As in the case of Fe the values become increasingly uncertain at higher temperatures, due to the short duration of the $\sqrt{t}$ regime. Figure 10 shows the fraction of helium released by atomic diffusion. Evaluation of Eq. (19) for surface diffusion is given in Fig. 11.

V. DISCUSSION

Above it has been shown that a reciprocal dependence of D_{He} on c_0 indicates a dissociative diffusion mechanism with preferential trapping at implantation-induced vacancies. The slopes of the Arrhenius plots (solid lines) in Figs. 4 and 9 then represent the dissociation energies.

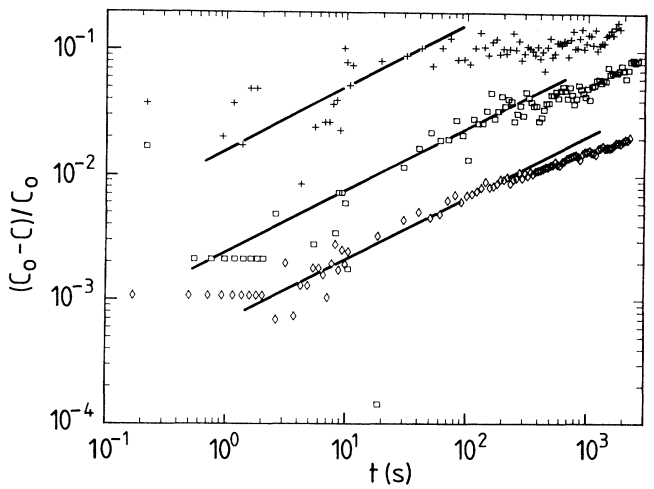

FIG. 3. Released fraction of implanted helium during isothermal degassing of iron. Temperatures (K), thicknesses (μm), and helium concentrations [at. ppm] were 559, 2.5, 1.39 (◇); 577, 20.6, 0.013 (□); and 667, 2.6, 0.109 (+), respectively.

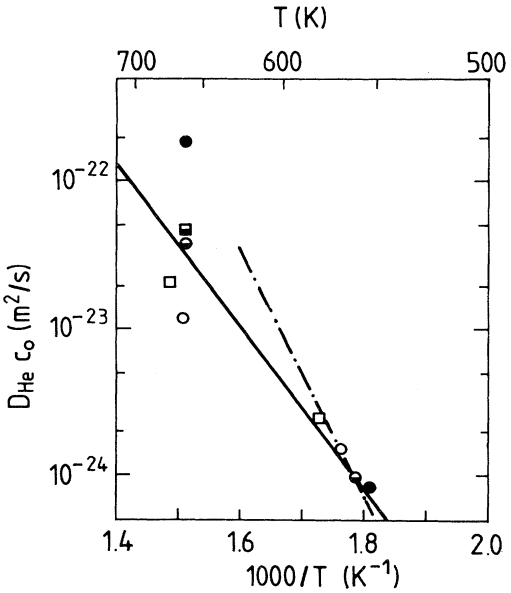

FIG. 4. Arrhenius plot of $D_{He}c_0$ of iron vs reciprocal temperature. Specimen thicknesses d (μm) and helium concentrations c_0 (at. ppm) were 2.5, 0.01, (○); 2.5, 0.1 (◒); 2.5, 1.0 (●); 22.0, 0.01 (□); and 22.0, 0.1 (◘), respectively. The solid line is a least-squares fit to all data, while the dash-dotted line fits the low-temperature data with a reasonable prefactor D_0c_0 (see text).

This gives for iron $E^{dis}=1.09\pm0.16$ eV with a prefactor $D_0c_0=10^{-14.2}$ m^2/s and for vanadium $E^{dis}=1.0\pm0.1$ eV and $D_0c_0=10^{-14.7}$ m^2/s. Both prefactors are by orders of magnitude smaller than expected from Eq. (3). For reasonable values of ν_0 (3×10^{12}/s), r_i (nearest-neighbor distance) and c_v/c_0 (10) a D_0c_0 value of $\approx1.2\times10^{-9}$ m^2/s is obtained. If this prefactor is fixed in the fit of the

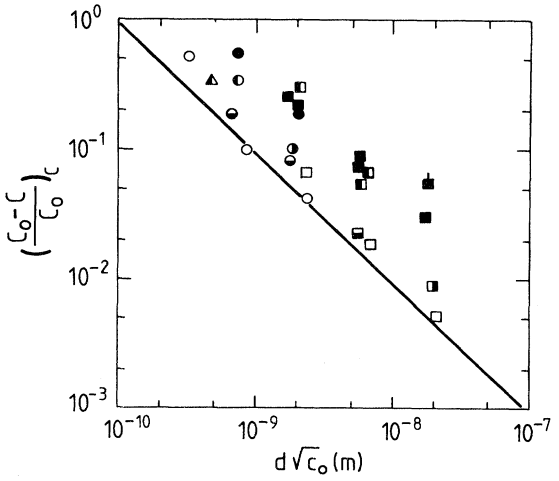

FIG. 5. Fraction of helium released from iron foils by atomic diffusion. Specimen thicknesses d (μm) and temperatures (K) were 2.5, 673 (○); 2.5, 873 (◒); 2.5, 1023 (◑); 2.5, 1123 (◐); 2.5, 1223 (●); 5.0, 1123 (◭); 22.0, 673 (□); 22.0, 873 (◘); 22.0, 1023 (◨); 22.0, 1123 (◧); 22.0, 1223 (■); and 22.0, 1323 (■), respectively. The solid line is expected if the helium is immobilized by the formation of stable di-helium complexes.

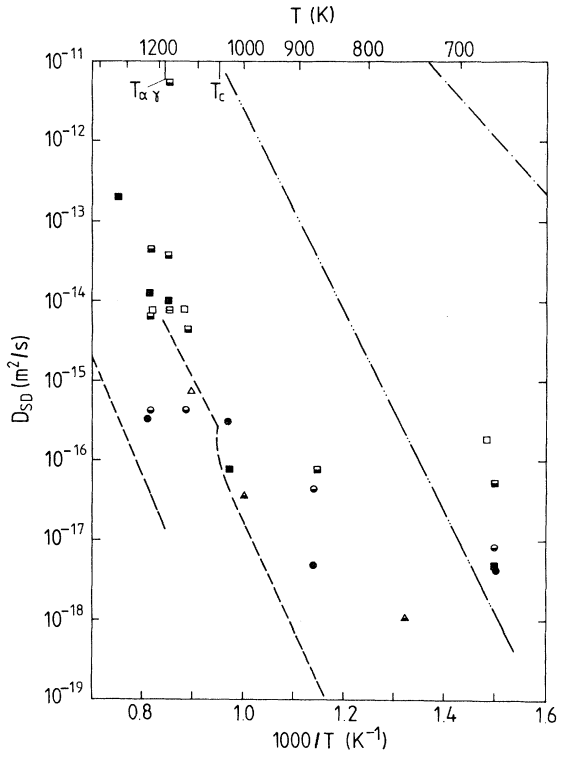

FIG. 6. Surface diffusion coefficients of iron determined from helium desorption experiments by Eq. (19), using $v_{He}=7.5\times10^{-30}$ m^3 and $r_0=0.15$ nm. Specimen thicknesses d (μm) and helium concentrations c_0 (at. ppm) where 2.5, 0.08 (◑); 2.5, 0.7 (●); 5.0, 0.01 (△); 5.0, 0.08 (◭); 5.0, 0.7 (▲); 22.0, 0.01 (□); 22.0, 0.08 (◘); and 22.0, 0.7 (■), respectively. The lines give literature data of volume (— —) and surface self-diffusion (—·—·—·) [17], (—··—) (see Ref. 18), respectively.

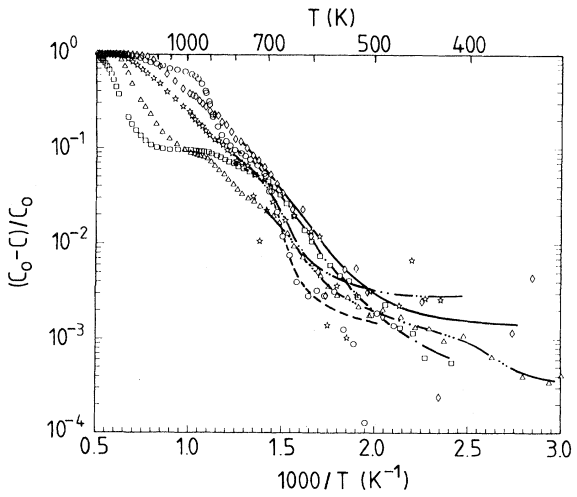

FIG. 7. Fractional release of implanted helium from vanadium foils during linear heating at a rate of 0.83 K/s. The specimens contained about 0.08 at. ppm He and had thicknesses (μm) of 4.5 (◇), 9.2 (○); 9.6 (*), 21 (□), and 43 (△), respectively.

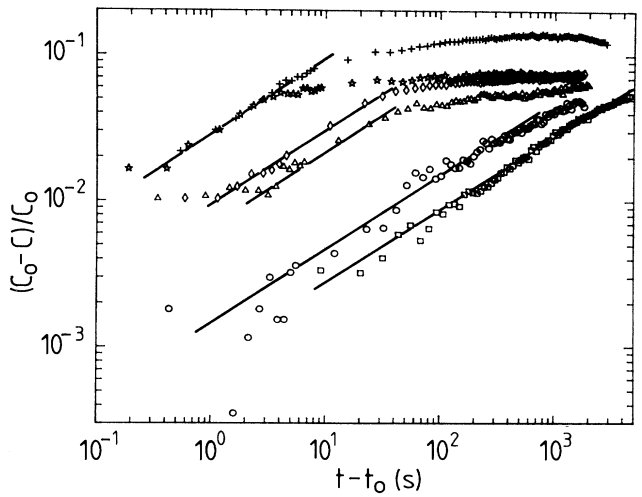

FIG. 8. Released fraction of implanted helium during isothermal degassing of vanadium, containing an initial helium concentration of about 0.02 at. ppm. Temperatures (K) and thicknesses (μm) were 575, 40.1 (□); 573, 21.5 (○); 672, 40.1 (◇); 674, 21.5 (△); 767, 40.1 (+); and 778, 21.5 (*), respectively. The time scales were corrected by values from 6 to 1 s (with increasing temperature) to account for heating time.

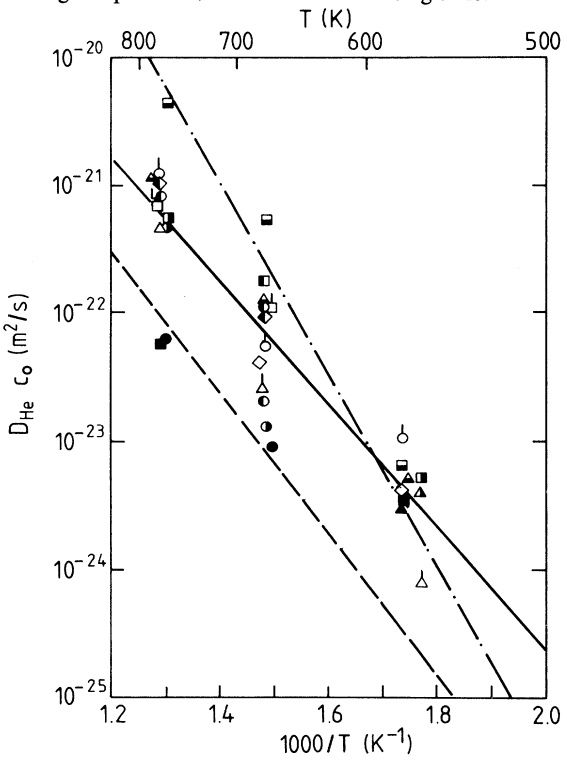

FIG. 9. Arrhenius plot of $D_{He}c_0$ of vanadium vs reciprocal temperature. Specimen thicknesses d (μm) and helium concentration (at. ppm) were 5, 0.001, (◇); 5, 0.08 (◈); 10, 0.007 (◌); 10, 0.08 (◐); 10, 0.3 (◍); 10, 3.5 (●); 20, 0.001 (△); 20, 0.007 (△); 20, 0.025 (▲); 20, 0.08 (▲); 20, 0.3 (▲); 20, 3.5 (▲); 41, 0.001 (□); 41, 0.007 (□); 41, 0.025 (□); 41, 0.08, (□); 41, 0.3 (□); and 41, 3.5 (■); respectively. The solid line is a least-squares fit to all data, while the dash-dotted line fits the low-temperature data with a reasonable prefactor D_0c_0 (see text). The dashed line gives values derived from linear heating experiments.

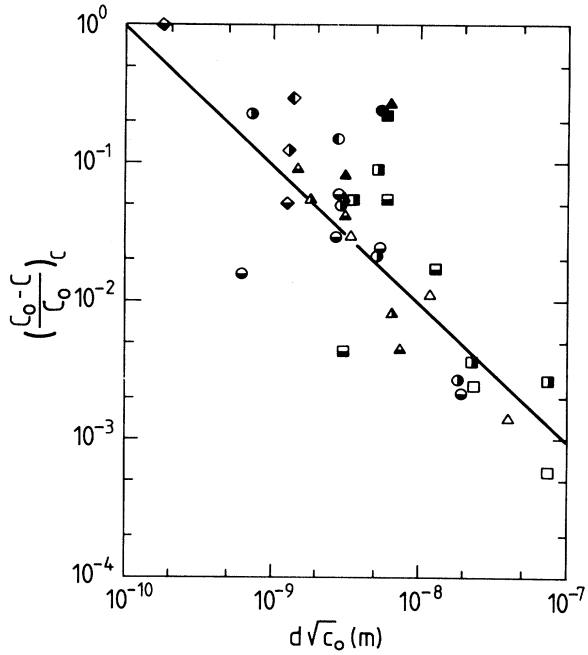

FIG. 10. Fraction of helium released from vanadium foils by atomic diffusion. Specimen thicknesses d (μm) and temperatures (K) were 5, 673 (◈); 5, 773 (◈); 5, 973 (◈); 9, 673 (◒); 9, 773 (◑); 9, 973 (◐); 9, 1173 (●); 21, 573 (△); 21, 673 (▲); 21, 773 (▲); 21, 1173 (▲); 40, 573 (□); 40, 673 (□); 40, 773 (□); 40, 1173 (■); respectively. The solid line is expected if the helium is immobilized by the formation of stable di-helium complexes.

low-temperature data where the $\sqrt{t}$ law is best established, the dash-dotted lines are obtained with $E^{dis}=1.68$ eV for iron and $E^{dis}=1.66$ eV for vanadium. These values are still far below dissociation energies derived from theoretical calculations,[13] which gave $E^{dis}(Fe)=3.1$ eV and $E^{dis}(V)=3.9$ eV, respectively.

The linear heating experiments on vanadium show steps at about 900 and 1500 K. At high He concentration an additional step at 600 K appears. Assuming first-order reactions, activation energies of 2.0, 2.7, and 3.9 eV, respectively, would correspond to these steps. At present these values cannot be assigned to specific dissociation processes.

In an experimental attempt to determine helium diffusion in iron (Lewis and Farrell[14]) and vanadium (Lewis[15]), 200 keV ^{3}He- ions were implanted at temperatures from 300 to 1064 K, and the implantation profiles were analyzed at room temperature by the ^{3}He(d,p)^{4}He reaction. For both metals a significant loss of helium was observed at elevated temperatures. Our results indicate that this is not due to diffusion of free helium but should be ascribed to helium losses during bubble coarsening. Bubbles form readily during implantation at the high average concentrations of about 0.2% used in these experiments.

From the data in Figs. 5 and 10 information on the stability of dihelium complexes can be obtained by comparison to Eq. (10). If the interatomic distance is used as a

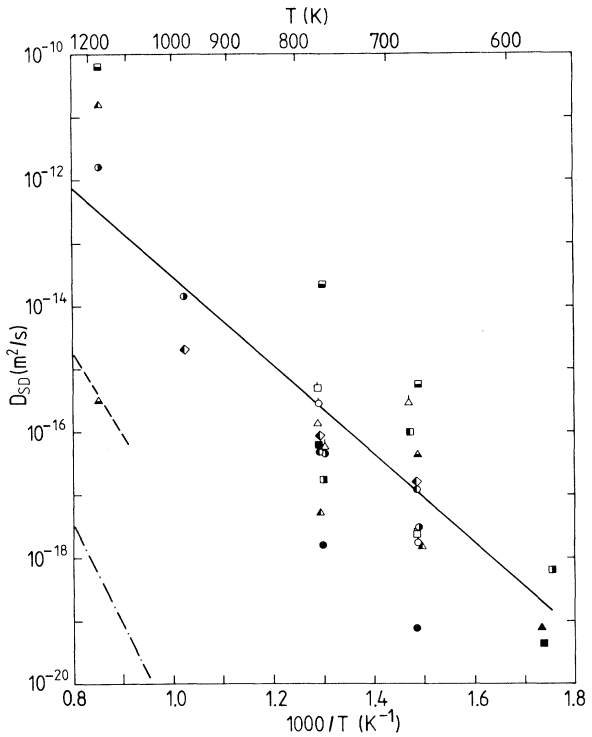

FIG. 11. Surface diffusion coefficients of vanadium determined from helium desorption experiments by Eq. (19), using $v_{He}=7.5\times10^{-30}$ m^3 and $r_0=0.15$ nm. Specimen thicknesses d (μm) and helium concentrations c_0 (at. ppm) were 5, 0.08 (◈); 10, 0.007 (◌); 10, 0.08 (◐); 10, 0.3 (◑); 10, 3.5 (●); 20, 0.001 (△); 20, 0.007 (△); 20, 0.025 (▲); 20, 0.08 (◭); 20, 3.5 (▲); 41, 0.007 (□); 41, 0.025 (▬); 41, 0.08 (◧); 41, 0.3 (◨); 41, 3.5 (■); respectively. The lines give surface diffusion coefficients derived from TEM studies on bubble coarsening (dashed line) (see Ref. 11) and volume self-diffusion (dash-dotted line).

lower limit for the interaction distance of helium atoms, the solid lines are obtained. For iron only the data points at 673 K; for vanadium those up to 773 K fall below or close to the line. This indicates that above this temperature di-helium complexes become unstable.

The sensitivity of the fit of Eq. (19) to the data after clustering suffers from slow desorption rates. For most specimens the amount of helium desorbing in this regime during typical measuring times of 1 h is smaller than that desorbed by free diffusion. In Figs. 6 and 11 the evaluation of Eq. (19) has been performed for surface diffusion, assuming constant volume per He atom ($v_{He}=7.5\times10^{-30}$ m^3) only. The initial bubble radius r_0 was set equal to 0.15 nm, which corresponds to a sphere containing two helium atoms. The diffusion coefficients would not be significantly altered by assuming an ideal gas law with a surface energy $\gamma_B=2$ N/m. The evaluation for volume diffusion gave D_v values which were by an almost constant factor of about 4 higher than the D_s values (compare B values in Table I). In spite of the rather large scattering of the data, comparison of the iron data to self-diffusion in Fig. 6 indicates that from about 900 to 1200 K volume diffusion controlled bubble migration to the surfaces of the specimen gives the best fit to the helium desorption data. At lower temperatures surface diffusion may contribute. On the other hand, in vanadium surface diffusion dominates over the whole temperature regime investigated. Transmission electron microscopy (TEM) in Ref. 11 also indicated surface diffusion as the dominant mechanism of bubble coarsening in vanadium. The surface diffusion coefficients derived in Ref. 11 are below the present values by about 2 orders of magnitude. On the other hand, activation energies E_{SD} from conventional surface diffusion measurements on bcc metals[16] roughly scale with the melting temperature T_M, giving values E_{SD}/kT_M of 8.5 (Nb), 9.7 (W), and 10.1 (Mo), which compare reasonably well with a value of 7.5 ($E_{SD}=1.4\pm0.2$ eV) derived from the data in Fig. 11 for vanadium.

VI. CONCLUSIONS

(1) The present study has shown that also in bcc metals very low helium concentrations are mandatory in studying atomic diffusion. This confirms previous results on fcc metals.[6]

(2) It was shown that quantitative information on the stability of small helium clusters can be inferred from the fraction of helium released by atomic diffusion.

(3) Calculations of helium desorption during bubble coarsening were performed and compared to experimental results. This enables helium desorption spectroscopy to study the coarsening of submicroscopic bubbles, which so far was only accessible to techniques like small-angle neutron scattering (SANS) or positron annihilation spectroscopy (PAS).

ACKNOWLEDGMENT

Part of this work was funded through the association EURATOM-KFA.

[1]J. F. Ziegler, *Helium Stopping Powers and Ranges in All Elements* (Pergamon, New York, 1978).
[2]P. Jung and V. Sciani, in *Diffusion in Metals and Alloys,* edited by F. J. Kedves and D. L. Beke (Trans Tech, 1983), p. 446.
[3]R. Vassen, RWTH Aachen Report No. Jül-2354, 1990 (unpublished).
[4]Proceedings of the International Symposium on Fundamental Aspects of Helium in Metals [Radiat. Eff. **78**, (1983)].
[5]H. S. Carslaw and J. C. Jaeger, *Conduction of Heat in Solids* (Clarendon Press, Oxford, 1959).
[6]V. Sciani and P. Jung, Radiat. Eff. **78**, 87 (1983).
[7]K. Schroeder, in *Point Defects in Metals II,* Vol. 87 of *Springer Tracts in Modern Physics* (Springer, Berlin, 1980), p. 171.
[8]P. Jung and K. Schroeder, J. Nucl. Mater. **155**, 1137 (1988).

[9]F. A. Nichols, J. Nucl. Mater. **30**, 143 (1969).
[10]E. E. Gruber, J. Appl. Phys. **38**, 243 (1966).
[11]P. J. Goodhew and S. K. Tyler, Proc. R. Soc. London, Ser. A **377**, 151 (1981).
[12]H. Trinkaus (unpublished).
[13]W. D. Wilson, in Conference on Fundamental Aspects of Radiation Damage in Metals, edited by F. W. Young and M. T. Robinson, Report No. USERDA-CONF-751006-P2, p. 1025.
[14]M. B. Lewis and K. Farrell, Nucl. Instrum. Methods Phys. Res. Sect. B **16**, 163 (1986).
[15]M. B. Lewis, J. Nucl. Mater. **152**, 114 (1988).
[16]H. P. Bonzel, in *Diffusion in Metals and Alloys,* Vol. XX of Landolt-Börnstein, edited by H. Mehrer (Springer Verlag, Berlin, in press).
[17]Y. E. Geguzin, G. N. Kovalor, and A. M. Ratner, Phys. Met. Metallogr. **10**, 45 (1960).
[18]J. M. Blakely and H. Mykura, Acta. Metall. **11**, 399 (1963).